

# Multi-band superconductivity and possible nodal gap in $\text{RbCr}_3\text{As}_3$ revealed by Andreev reflection and single-particle tunneling measurements

Zhixin Liu,<sup>1</sup> Mingyang Chen,<sup>1</sup> Ying Xiang,<sup>1</sup> Xiaoyu Chen,<sup>1</sup> Huan Yang,<sup>1,\*</sup> Tong

Liu,<sup>2,3,4</sup> Qing-Ge Mu,<sup>2,3,4</sup> Kang Zhao,<sup>2,3,4</sup> Zhi-An Ren,<sup>2,3,4</sup> and Hai-Hu Wen<sup>1,†</sup>

<sup>1</sup>*National Laboratory of Solid State Microstructures and Department of Physics,*

*Collaborative Innovation Center of Advanced Microstructures, Nanjing University, Nanjing 210093, China*

<sup>2</sup>*Beijing National Laboratory for Condensed Matter Physics,*

*Institute of Physics, Chinese Academy of Sciences, Beijing 100190, China*

<sup>3</sup>*School of Physical Sciences, University of Chinese Academy of Sciences, Beijing 100190, China and*

<sup>4</sup>*Collaborative Innovation Center of Quantum Matter, Beijing 100190, China*

By measuring point-contact Andreev reflection spectra in the newly discovered chromium-based quasi-one-dimensional superconductor  $\text{RbCr}_3\text{As}_3$ , we find clear evidence of two superconducting components, one has a gap value of about 1.8 meV and another about 5 meV. Detailed analysis finds that the larger gap possesses an  $s$ -wave nature, but the smaller gap exhibits a sharp peak feature near zero energy on the Andreev reflection spectrum manifesting a possible nodal gap. We then carry out the single-particle tunneling measurements based on a scanning tunneling spectroscopy (STS) by using the needle-like sample as the tip, and in this case the measuring current is parallel to the  $k_z$  or  $[(\text{Cr}_3\text{As}_3)^-]_\infty$ -chain direction. The single-particle tunneling spectra show only one gap feature with the gap value of about 1.8 meV. Fitting to the single particle tunneling spectra tells that the gap should have a large anisotropy or even node(s). We argue that the smaller gap may be mainly contributed by the hybridized Fermi surface with a large weight coming from the quasi-1D bands. Therefore our results from combinatorial experiments of Andreev reflection and STS are consistent with the theoretical predictions for multi-band superconductivity and a possible  $p$ -wave superconducting gap along the  $[(\text{Cr}_3\text{As}_3)^-]_\infty$ -chain direction.

## I. INTRODUCTION

In materials containing 3d transition-metal elements, many new superconductors have been discovered and some of them show the unconventional superconductivity. The latter is argued to have a close relationship with the strong correlation effect of electrons in the 3d orbital. For the compounds containing 3d transition metal chromium, superconductivity was first observed in the binary CrAs under pressure with a transition temperature  $T_c \sim 2$  K [1]. After that some new quasi-one-dimensional (quasi-1D) Cr-based superconductors were discovered at ambient pressure, and they are mainly classified to two families including 233 and 133 with the chemical formulas of  $A_2\text{Cr}_3\text{As}_3$  and  $A\text{Cr}_3\text{As}_3$  ( $A = \text{K}, \text{Rb}, \text{Cs}$ ), respectively [2–6]. Recently, the superconductor  $\text{Na}_2\text{Cr}_3\text{As}_3$  was also successfully synthesized [7], and it has the highest  $T_c = 8.6$  K among these Cr-based superconductors. This discovery has been extended to the Mo-based system, superconductivity with  $T_c$  of about 10.3 K has been reported in  $\text{K}_2\text{Mo}_3\text{As}_3$  [8]. It has been claimed that the 133 phase may be more stable against water moisture in air, thus it is more easy to be handled for many elegant measurements. The structural characteristic of the Cr-based materials is that it contains the 1D  $[(\text{Cr}_3\text{As}_3)_\infty^-]$  chains separated by alkali metal atoms [2], which makes the physical properties and superconductivity of these materials more interesting.

Clearly, the newly discovered Cr-based superconductors provide a new platform to research on the superconductivity related to the pairing of 3d electrons. The band structure calculations of  $A_2\text{Cr}_3\text{As}_3$  reveal three sets

of Fermi surfaces (FSs) which are mainly contributed by 3d orbitals of chromium. The FSs consist of two flat ones from quasi-1D  $\alpha$  and  $\beta$ -bands as well as a three-dimensional (3D) one from 3D  $\gamma$ -band [9–12]. The quasi-1D FSs were then confirmed by angle-resolved photoemission spectroscopy measurements in  $\text{K}_2\text{Cr}_3\text{As}_3$  [13]. Because of the complex band structure, different kinds of unconventional pairing symmetries were predicted for  $A_2\text{Cr}_3\text{As}_3$  superconductors theoretically. One interesting proposal is the nodal triplet  $p_z$ -wave pairing which is dominated by the quasi-1D  $\beta$  band and driven by the ferromagnetic fluctuations within the Cr sublattice [11]. Another prediction is that the pairing can change from a spin-triplet state  $f_{y(3x^2-y^2)}$  with line nodes at the 3D  $\gamma$ -band to a spin-triplet fully gapped state  $p_z\hat{z}$  at the quasi-1D  $\alpha$ -band when the strength ratio between Hund's coupling and inter-orbital repulsion decreases [12]. Meanwhile from some other theoretical works, the quasi-1D and 3D FSs may couple with each other, which results in a strongly anisotropic singlet pairing and gap nodal rings on the 3D Fermi sphere when the local repulsion is strong enough [14].

Up to now many experimental results suggest unconventional superconductivity in  $A_2\text{Cr}_3\text{As}_3$ . The very large upper critical field  $H_{c2}$  exceeding the Pauli limit may suggest a strong and unconventional pairing mechanism [2, 3, 15, 16]. Furthermore, in  $\text{K}_2\text{Cr}_3\text{As}_3$ , it was found that  $T_c$  decreases significantly with increase of the density of non-magnetic impurities, which may suggest the sign-reversal gaps of superconductivity [17]. The similar conclusions have also been obtained from the absence of the Hebel-Slichter coherence peak of  $1/T_1$  just below

$T_c$  in NMR studies [18, 19]. In addition,  $1/T_1$  decreases rapidly below  $T_c$  following a function of  $T^5$  at low temperatures in  $\text{Rb}_2\text{Cr}_3\text{As}_3$ , which may be a proof of the presence of point nodes in the gap function [19]. The possible line-nodal gap was proved by low-temperature electronic specific-heat data [20] and the  $\mu\text{SR}$  data [21] in  $\text{K}_2\text{Cr}_3\text{As}_3$ , as well as the penetration depth measurements in  $\text{K}_2\text{Cr}_3\text{As}_3$  and  $\text{Rb}_2\text{Cr}_3\text{As}_3$  [22]. The anisotropic superconductivity was observed in  $A_2\text{Cr}_3\text{As}_3$  not only when the magnetic field is applied along or perpendicular to the  $c$ -axis, but also with the in-plane rotation of field [15], and the threefold in-plane  $H_{c2}$  modulation was observed and was argued to be related to the spin-triplet pairing [23].

The  $A\text{Cr}_3\text{As}_3$  family has half amount of the alkali metal atoms comparing to the  $A_2\text{Cr}_3\text{As}_3$  family, and the space groups for these two families are different [5, 6]. However, they both contain the 1D  $[\text{Cr}_3\text{As}_3]_\infty$  chains but with different ionic valences of the  $\text{Cr}_3\text{As}_3$  units. The normal-state electrical resistivity also has different temperature dependent behaviors in these two families of the materials [5, 6]. Theoretical calculation predicted that FSs are constructed by two or three quasi-1D and two 3D bands [24, 25], and superconducting pairing symmetry can be triplet  $f$ -,  $p_z$ - or singlet  $s^\pm$ -wave with different interaction parameters [25]. The nodal superconducting gap structure in  $\text{RbCr}_3\text{As}_3$  was inferred from the thermal conductivity measurements which show a sizable value of the thermal conductivity coefficient in the zero temperature limit at ambient field, and the magnetic field enhancement is clearly faster than that expected for a full-gap superconductor [26]. However, more experiments are required to derive the information of the superconducting gap in the Cr-based family.

Andreev reflection and single-particle tunneling measurements are very useful and combinatorial to detect the superconducting gap. In this work, we will present a detailed study of the superconducting gap structure on the  $\text{RbCr}_3\text{As}_3$  single crystals by using the point-contact Andreev reflection (PCAR) and scanning tunneling spectroscopy (STS) measurements. The results show the existence of two superconducting components. The large gap has the value of about 5 meV, and shows only on the Andreev reflection spectra measured when the injecting current is mainly perpendicular to the  $c$ -axis; while the smaller one with the value of about 1.8 meV can be observed both on the Andreev reflection and the STS measurements when the injecting current is along the  $c$ -axis. We suggest that the smaller gap is highly anisotropic or even has nodes based on the fitting to the STS data.

## II. EXPERIMENTAL METHODS AND SUPERCONDUCTIVITY CHARACTERIZATION

The  $\text{RbCr}_3\text{As}_3$  single crystals were grown by the deintercalation process of  $\text{Rb}^+$  ions from  $\text{Rb}_2\text{Cr}_3\text{As}_3$  precursors [6]. The samples are loosely assembled by many

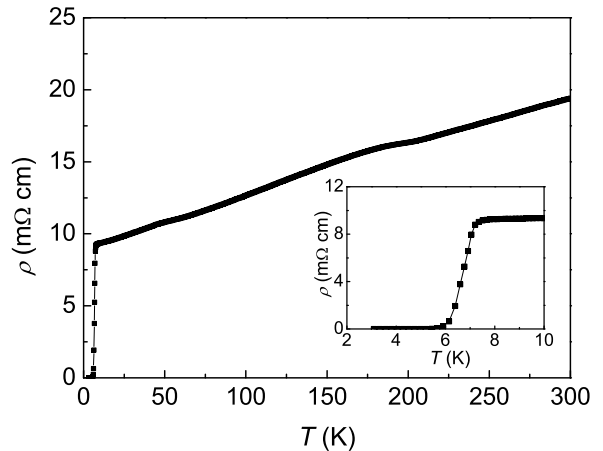


FIG. 1. Temperature dependence of resistivity of a  $\text{RbCr}_3\text{As}_3$  sample. The inset shows the enlarged view of the  $\rho$ - $T$  curve near the superconducting transition.

needle-like single crystals with diameter of sub- to several micrometers, and they are stable in the air. The electrical resistivity was measured in a physical property measurement system (PPMS-9, Quantum Design) by using the standard four-probe method, and the current is applied along the  $c$ -axis of the sample. Figure 1 shows the temperature dependent resistivity for a  $\text{RbCr}_3\text{As}_3$  sample at 0 T, and the inset shows the enlarged view near the superconducting transition. The onset transition temperature  $T_c$  is 7.06 K determined from the 90% of the normal-state resistivity, and the transition width is about 0.87 K determined by using criterion of 10% and 90% normal-state resistivity. The residual resistance ratio  $RRR = \rho(300 \text{ K})/\rho(8 \text{ K} > T_c) = 2.1$  is consistent with previous report in  $\text{RbCr}_3\text{As}_3$  but much smaller than the obtained value in  $\text{Rb}_2\text{Cr}_3\text{As}_3$  [3, 6].

The samples for PCAR or STS measurements are divided from the initial bundle of the sample, and the typical sizes of selected samples are 300-500  $\mu\text{m}$  in length and about several micrometers in width. For the PCAR measurements, the point contact was constructed by sticking a thin gold wire with the diameter of 16  $\mu\text{m}$  to the sample by using a tiny bit of silver paste (DuPont, 4929N), and a typical configuration is shown in the inset of Fig. 2(a). The injecting current is mainly along  $ab$ -plane of the sample during the PCAR measurements. The length of the sample in the point-contact region was about 20  $\mu\text{m}$ , and the two ends of the sample were buried in the silver paste with more than one hundred micrometers in length to reduce the contact resistance of these electrodes. Since the contact constructed by silver paste has a finite size, the current may have a bit of component in the direction parallel to the  $[(\text{Cr}_3\text{As}_3)^-]_\infty$ -chains. The measured resistance of the point contact was about several dozens

of ohms. The PCAR measurements were carried out in PPMS-9 by using a home-made setup. The ac modulation for the differential conductance measurement is several microamperes with the frequency of 985 Hz in the lock-in measurements.

The STS measurements were carried out in an ultra-high vacuum, low-temperature and high-magnetic field scanning tunnelling microscope (USM-1300, Unisoku Co., Ltd.). The sample is used as the STS tip, and the tip is made by following steps. We first found a very thin wire of the sample by tweezers, and then cut off one end to get a relatively fresh terminal for the STS tip. Afterwards, we used the silver paste to glue most part of the sample on a Pt/Ir tip, and made the newly-cut prominent end face towards the Au surface as the tip for the STS measurement. The single-particle tunneling spectra were recorded between the needle-like sample tip and a flat Au(111) single-crystal flake sample (purity 99.999%) in an ultra-high vacuum chamber with a base pressure of about  $1 \times 10^{-10}$  torr. The direction of injecting current is along the  $[(\text{Cr}_3\text{As}_3)^-]_\infty$ -chain direction or  $c$ -axis of the sample for the STS measurements. The setpoint condition for the spectrum measurements is  $I_{set} = 50$  pA and  $V_{set} = 10$  mV, and the ac modulation is 0.5 mV with the frequency of 871.773 Hz.

### III. POINT-CONTACT ANDREEV REFLECTION RESULTS

Figure 2(a) shows the measured PCAR spectra at different temperatures and 0 T. One can see that there are always zero-bias peaks on the spectra taken below  $T_c$ . This kind of peak appears quite often in the PCAR measurements on an unconventional superconductor, especially when the injecting current is along the nodal direction. In cuprate superconductors, this has been well investigated both in theory [27–29] and experiments [30–32]. It should be noted that there are a pair of kink features at about  $\pm 5$  meV on the spectrum measured at 3 K, and they are marked by black arrows in Fig. 2(a). We will show through fitting that this corresponds to the second superconducting gap in  $\text{RbCr}_3\text{As}_3$ . Beside the superconducting gap features, some unexpected small dips of  $dI/dV$  can be also observed at low temperatures and energies just above the superconducting gap energy, e.g., at energies from 10 to 15 meV for the spectrum measured at 3 K. The bottom energies of these dips decrease with increase of temperature. This kind of dip feature seems to be very common in point-contact measurements and was argued to be induced by the critical current effect or the heating effect when the voltage is high and the point contact is not in the pure ballistic limit [33]. From temperature dependence of the spectra, one can see that the height of the zero-bias peak decreases with increase of temperature, and the spectrum changes to a ‘V’-shape normal-state background when the temperature reaches 7 K  $\sim T_c$ . To get rid of the background signal, we nor-

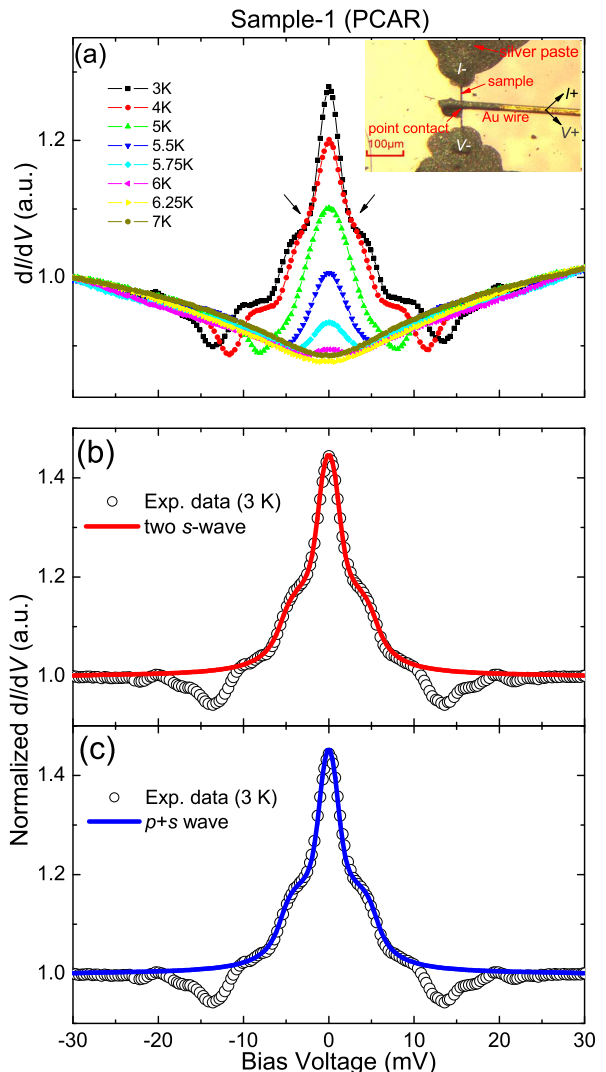


FIG. 2. (a) Raw data of PCAR spectra measured at various temperatures in  $\text{RbCr}_3\text{As}_3$  Sample-1. The inset shows the photograph of the point-contact junction for the Andreev reflection measurement. The point contact is constructed by a little bit of silver paste attaching to a gold wire with the diameter of 16  $\mu\text{m}$ , and two ends of the sample are buried in the silver paste in order to lower down the contacting resistance. The junction resistance is about 159  $\Omega$  at 3 K. (b) Normalized PCAR spectra (open circles) at 3 K divided by the one at 7 K, and the BTK fitting result (the solid line) with two isotropic  $s$ -wave gaps. The obtained gap values are  $\Delta_{s1} = 1.1$  meV and  $\Delta_{s2} = 5$  meV; the other fitting parameters are  $w_1 = 0.75$ ,  $\Gamma_{s1} = 0.46$  meV,  $\Gamma_{s2} = 0.65$  meV, and  $Z_{s1} = Z_{s2} = 0.1$ . (c) Normalized PCAR spectra (open circles) at 3 K and the BTK fitting result (the solid line) by a  $p$ -wave and an isotropic- $s$ -wave gap ( $\Delta_{p1} = 1.4 \sin \theta$  meV,  $\Delta_{s2} = 5$  meV). The other fitting parameters are  $w_1 = 0.75$ ,  $\Gamma_{p1} = 0.39$  meV,  $\Gamma_{s2} = 0.65$  meV, and  $Z_{p1} = Z_{s2} = 0.1$ .

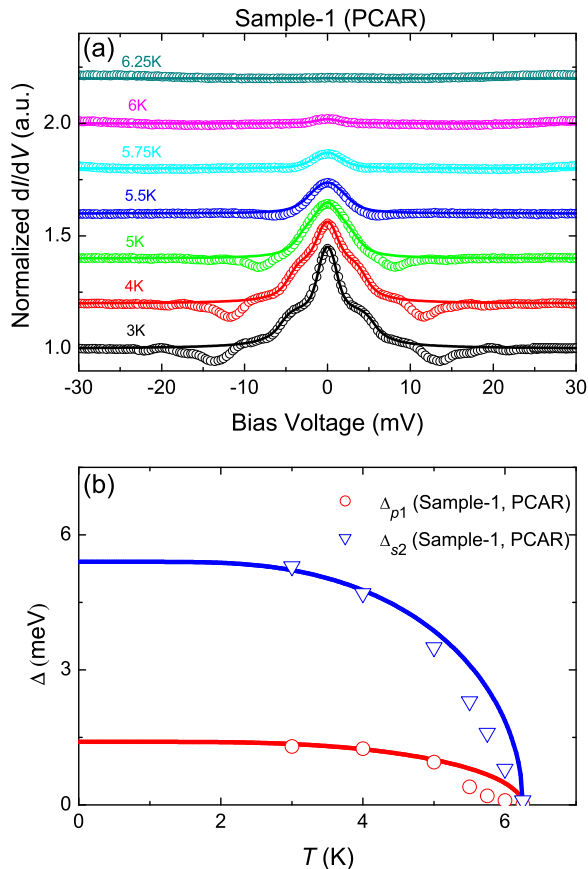


FIG. 3. (a) The normalized PCAR spectra (open circles) divided by the spectrum measured at 7 K, and the two-band BTK fitting results (solid lines) by using a  $p$ -wave and an isotropic- $s$ -wave gap. The fitting parameters  $w_1 = 0.75$  and  $Z_1 = Z_2 = 0.1$  keep constant for all the spectra at different temperatures, while  $\Gamma_1$  and  $\Gamma_2$  change slightly with increase of temperature. (b) Temperature dependence of the superconducting gaps from fitting results (open symbols) for Sample-1, and the solid lines are the theoretical curves from the weak-coupling BCS model.

malized the spectrum measured at 3 K by dividing the one measured at 7 K, and the normalized curve is shown by the open circles in Fig. 2(b) and 2(c). The differential conductance at zero-bias is about 1.45 times larger than the value of the high-energy normal-state background for the normalized spectrum at 3 K, which suggests that the barrier height of the junction is small and the contribution from the Andreev reflection is much larger than that from single-particle tunneling.

In order to get in-depth understanding of superconducting gaps from the PCAR spectra, we fit the data with the Blonder-Tinkham-Klapwijk (BTK) theory [34]. The expression of differential conductance  $G = dI/dV$

from BTK theory reads,

$$G(V) = \int_{-\infty}^{+\infty} \frac{df(E-V, T)}{dV} [1 + A(E) - B(E)] dE, \quad (1)$$

where  $f(E, T)$  is the Fermi distribution function, and  $A(E)$  and  $B(E)$  represent the contributions from the Andreev reflection and single-particle tunneling, respectively. Then the PCAR spectra can be described by the superconducting gap  $\Delta$ , the junction barrier height  $Z$ , the broadening factor  $\Gamma$ , and temperature  $T$  [29]. Since there is an obvious two-gap feature on the PCAR spectrum measured at 3 K, we use a two-gap BTK model [35] to fit the normalized differential conductance  $G$  as

$$G = w_1 G_1 + (1 - w_1) G_2. \quad (2)$$

Here  $w_1$  is the weight for the smaller gap, and  $G_1$  and  $G_2$  are the normalized differential conductances originated from different bands with smaller and larger superconducting gaps, respectively. The BTK fitting results by two isotropic  $s$ -wave gaps and  $p$ + $s$  wave gaps are shown in Fig. 2(b) and 2(c). It is found that the PCAR spectra can be well fitted by the BTK model. Here for the  $p$ -wave gap, we use the gap function of  $\Delta_p \sin \theta$ . One can see that the fitting results are similar to each other with two different kinds of superconducting gap functions for the component with smaller gap. Therefore, purely from the fitting to the PCAR spectra, we can not make judgement whether the smaller gap has the gap nodes. For the conclusion of a possible nodal gap, we will combine with the STS measurements shown later. For the larger gap, one can see a pair of shoulders, which according to the fitting suggests a full gap. From these fittings, we find that the system contains two superconducting components, one with a smaller gap with the maximum magnitude of about 1.4 meV may be nodal-like, another one with larger gap value of 5 meV has a full gap feature. In order to obtain the temperature dependent behavior of the superconducting gap, we use the two-gap BTK model with a  $p$ -wave gap and an isotropic  $s$ -wave gap to fit the normalized PCAR spectra at different temperatures, and the fitting results are shown in Fig. 3(a). Figure 3(b) shows the obtained temperature dependence of the two superconducting gaps derived from the fitting. The solid lines are the theoretical calculations carried out by using the Bardeen-Cooper-Schrieffer (BCS) gap model.

In order to verify our experimental results, we carried out the PCAR experiments on different samples, and the data for two other samples are shown in Fig. 4. The normalized spectra measured in Sample-2 and Sample-3 show the similar two-gap features as in Sample-1, but with slightly different gap values. In this point of view, the two-gap nature is verified by measurements on different point-contact junctions with various junction resistances. Besides, the spectrum weight from the band(s) with smaller gap is much larger than that with the larger gap, and the weight ratios are all about 3:1.

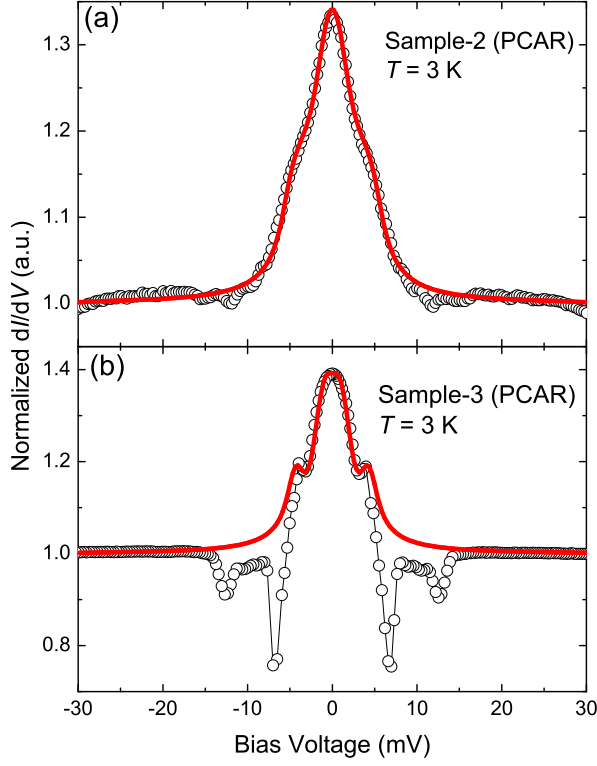


FIG. 4. (a) The normalized PCAR spectrum for Sample-2 (open circles) and the two-gap ( $p+s$  waves) BTK fitting result (the solid line) at 3 K. The resistance of the point-contact junction is about  $17 \Omega$ . The fitting parameters are  $\Delta_{p1} = 1.8 \sin \theta$  meV,  $\Delta_{s2} = 5.3$  meV,  $w_1 = 0.75$ ,  $\Gamma_{p1} = 0.9$  meV,  $\Gamma_{s2} = 0.7$  meV, and  $Z_{p1} = Z_{s2} = 0.1$ . (b) The normalized PCAR spectrum for Sample-3 (open circles) and the BTK fitting curve by  $p+s$  wave gap (the solid line) at 3 K. The junction resistance is about  $4 \Omega$ . The fitting parameters are  $\Delta_{p1} = 2.2 \sin \theta$  meV,  $\Delta_{s2} = 4.5$  meV,  $w_1 = 0.75$ ,  $\Gamma_{p1} = 0.32$  meV,  $\Gamma_{s2} = 0.35$  meV,  $Z_{p1} = 0.28$ , and  $Z_{s2} = 0.75$ .

#### IV. SCANNING TUNNELING SPECTROSCOPY RESULTS

The Andreev reflection results presented above clearly show the two superconducting-gap features. However, we can not judge whether these gaps are nodal or nodeless because the lowest measurement temperature is only 3 K. We then do the further measurements by STS at temperature as low as 400 mK. The needle-like sample, which was attached to the end of the Pt/Ir tip, was used as the tip for the STS measurements. The tunneling spectra were taken between the sample and a flat gold flake as illustrated by the schematic figure in the inset of Fig. 5(a). In this configuration, the tunneling current is predominantly along the  $k_z$  direction of the  $\text{RbCr}_3\text{As}_3$  crystal. The tunneling spectra measured at 400 mK and above  $T_c$  are displayed in Fig. 5(a) and 5(e) for Sample-4

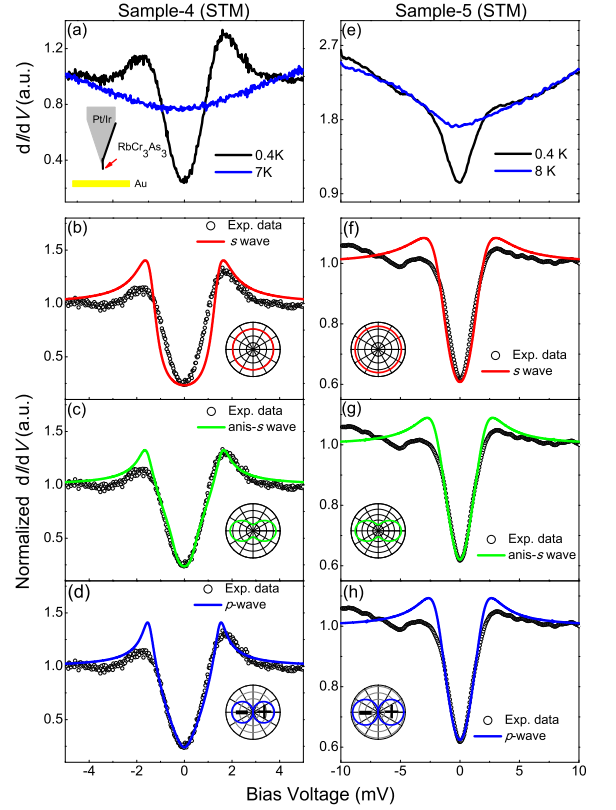


FIG. 5. The measured STS spectra at 400 mK and above  $T_c$  for (a) Sample-4 and (e) Sample-5. The inset in (a) displays the schematic configuration of STS measurements, and the tunneling spectra are taken between the needle-like sample of  $\text{RbCr}_3\text{As}_3$  attached to the Pt/Ir tip and a flat gold flake with the junction resistance of about  $0.2 \text{ G}\Omega$ . Normalized STS spectra (open circles) at 400 mK and the Dynes model fitting results (solid lines) by different gap functions for (b-d) Sample-4 and (f-h) Sample-5. The superconducting gap function used for the fitting are plotted in the insets of (b-d) and (f-h). The fitting parameters are (b)  $\Delta_s = 1.38$  meV, and  $\Gamma_s = 0.33$  meV; (c)  $\Delta_{ani-s} = 1.5(0.37 \cos \theta + 0.63)$  meV, and  $\Gamma_{ani-s} = 0.2$  meV; (d)  $\Delta_p = 1.5 \sin \theta$  meV, and  $\Gamma_p = 0.15$  meV; (f)  $\Delta_s = 1.7$  meV, and  $\Gamma_s = 1.3$  meV; (g)  $\Delta_{ani-s} = 2.12(0.37 \cos \theta + 0.63)$  meV, and  $\Gamma_{ani-s} = 0.98$  meV; (h)  $\Delta_p = 2.0 \sin \theta$  meV, and  $\Gamma_p = 0.94$  meV.

and Sample-5, respectively. One can see that the normal state spectra show a ‘V’-shape feature, which is somewhat similar to the normal-state background obtained by PCAR measurements. In addition, the superconducting spectra are of the typical single-particle tunneling type with only one pair of coherence peaks for both samples, which means that we detect mainly the contribution from one superconducting component. We use the spectra measured above  $T_c$  as the background and show the normalized spectra at 400 mK in Fig. 5(b-d) and 5(f-h) for two samples. Then the Dynes model [36] was used

to fit the normalized spectra by different kinds of gap functions, and the results are also shown in Fig. 5(b-d) and 5(f-h) as solid lines. Obviously, for an isotropic  $s$ -wave gap, the fitting cannot catch up the main features of the measured spectra for both samples; while the fitting results are much better for the anisotropic  $s$ -wave gap with a gap anisotropy of  $\Delta_{max}/\Delta_{min} = 3.8$  or the  $p$ -wave gap. A normalized zero-bias conductance ranging from about 0.3 to 0.6 can be seen in the spectra, which may be attributed to the impurity scattering effect for a nodal superconductor. Of course they can also be induced by the imperfection of the tip which contains a bundle of chain-like samples and a large scattering effect is inevitable. Although the origin for the zero bias conductance is unclear yet, we confidently conclude that the gap anisotropy is necessary for the fitting process.

## V. DISCUSSION AND CONCLUSION

From two different tunneling measurements, namely PCAR and STS, we find different numbers of contributions for superconductivity. In the PCAR measurements, two gaps are derived but only one gap is obtained from the STS measurements. Since the smaller gap feature exists in both cases with quite close values, they should have the same origin, namely, the smaller gap is highly anisotropic or even nodal. For the STS measurements, since the injecting current is mainly along the  $k_z$  direction, we would argue that the smaller gap exhibited on the STS spectra is originated from the 1D bands[11, 24]. From the theoretical calculations for  $A_2Cr_3As_3$  [11, 14] system, the quasi-1D FSs can couple with the 3D one and form a complex 3D FS, but the conduction along  $k_z$  direction is still dominated by the 1D bands. In this hybridized picture, the Fermi surface should be continuous in the momentum space, and the line nodes may exist on the central 3D Fermi pockets near  $k_z = 0$  [11, 14]. In our point of view, this newly hybridized 3D FS can be the origin of the smaller anisotropic or nodal gap in  $RbCr_3As_3$ . According to the theoretical calculation in  $ACr_3As_3$  [24, 25], another 3D FS exists, we would argue that the larger gap may accommodate on this FS. For the smaller gap with large anisotropy or even nodes, we regard it as a  $p$ -wave gap following the theoretical predictions. The gap values from the fittings to the spec-

tra measured in different samples are listed in Tab. I. Here for the smaller  $p$ -wave gap, the average gap value is  $\overline{\Delta}_p = 1.78 \pm 0.33$  meV, and the calculated gap ratio is  $2\overline{\Delta}_p/k_B T_c = 5.8 \pm 1.2$ . This value is much larger than 3.53 from weak coupling BCS theory. For the large  $s$ -wave gap  $\overline{\Delta}_s = 4.9$  meV, it corresponds to a huge ratio of  $2\overline{\Delta}_s/k_B T_c \approx 16$ . The large values of the gap ratio suggest the strong coupling and unconventional superconductivity in this material.

In summary, we observe two-gap feature from PCAR measurements in  $RbCr_3As_3$ , and the maximum gap values are about 1.8 and 5 meV. The smaller gap may be

TABLE I. The obtained superconducting gap values of  $RbCr_3As_3$  from fitting results of the measured PCAR and STS data.

Sample No.	PCAR (3K)			STS (400mK)	
	Sample1	Sample2	Sample3	Sample4	Sample5
$\Delta_p$ (meV)	1.4	1.8	2.2	1.5	2.0
$\Delta_s$ (meV)	5	5.3	4.5	-	-

highly anisotropic or even with gap nodes inferred from both the PCAR and STS measurements. Since we use the needle-like  $RbCr_3As_3$  sample as the tip for STS measurements and the injecting current is mainly along the  $k_z$  direction, we conclude that the smaller gap may open on the hybridized 3D Fermi surface constructed by the 1D bands and a 3D band. The large ratio of gap over  $T_c$ ,  $2\overline{\Delta}_s/k_B T_c \approx 16$ , clearly indicates pairing with a strong coupling. These observations are consistent with the theoretical predictions for a possible  $p$ -wave gap, and will stimulate further efforts in understanding the unconventional superconductivity in the family of Cr-based superconductors.

## ACKNOWLEDGMENTS

We appreciate the kind help in the PCAR measurements by Cong Ren, Lei Shan and Xingyuan Hou. This work was supported by National Key R&D Program of China (grant number: 2016YFA0300401), National Natural Science Foundation of China (grant number: 11534005).

\* huanyang@nju.edu.cn

† hhwen@nju.edu.cn

- 
- [1] W. Wei, J. G. Cheng, K. Matsubayashi, P. P. Kong, F. K. Lin, C. Q. Jin, N. L. Wang, Y. Uwatoko, and J. L. Luo, Nat. Commun. **5**, 5508 (2014).
- [2] J. K. Bao, J. Y. Liu, C. W. Ma, Z. H. Meng, Z. T. Tang, Y. L. Sun, H. F. Zhai, H. Jiang, H. Bai, C. M. Feng, Z. A. Xu, and G. H. Cao, Phys. Rev. X. **5**, 011013 (2015).
- [3] Z. T. Tang, J. K. Bao, Y. Liu, Y. L. Sun, A. Ablimit, H. F. Zhai, H. Jiang, C. M. Feng, Z. A. Xu, and G. H. Cao, Phys. Rev. B. **91**, 020506(R) (2015).
- [4] Z. T. Tang, J. K. Bao, Z. Wang, H. Bai, H. Jiang, Y. Liu, H. F. Zhai, C. M. Feng, Z. A. Xu, and G. H. Cao, Sci. China. Mater. **58**, 16 (2015).
- [5] Q. G. Mu, B. B. Ruan, B. J. Pan, T. Liu, J. Yu, K. Zhao, G. F. Chen, and Z. A. Ren, Phys. Rev. B. **96**, 140504(R) (2017).
- [6] T. Liu, Q. G. Mu, B. J. Pan, J. Yu, B. B. Ruan, K. Zhao, G. F. Chen, and Z. A. Ren, Europhys. Lett. **120**, 27006 (2018).

- [7] Q. G. Mu, B. B. Ruan, B. J. Pan, T. Liu, J. Yu, K. Zhao, G. F. Chen, and Z. A. Ren, *Phys. Rev. Mater.* **2**, 034803 (2018).
- [8] Q.-G. Mu, B.-B. Ruan, K. Zhao, B.-J. Pan, T. Liu, L. Shan, G.-F. Chen, Z.-A. Ren, *Sci. Bull.* **63**, 952 (2018).
- [9] H. Jiang, G. H. Cao, and C. Cao, *Sci. Rep.* **5**, 16054 (2015).
- [10] H. T. Zhong, X. Y. Feng, H. Chen, and J. H. Dai, *Phys. Rev. Lett.* **115**, 227001 (2015).
- [11] X. X. Wu, F. Yang, C. C. Le, H. Fan, and J. P. Hu, *Phys. Rev. B* **92**, 104511 (2015).
- [12] Y. Zhou, C. Cao, and F. C. Zhang, *Sci. Bull.* **62**, 208 (2017).
- [13] M. D. Watson, Y. Feng, C. W. Nicholson, C. Monney, J. M. Riley, H. Iwasawa, K. Refson, V. Sacksteder, D. T. Adroja, J. Zhao, and M. Hoesch, *Phys. Rev. Lett.* **118**, 097002 (2017).
- [14] G. Wachtel and Y. B. Kim, *Phys. Rev. B* **94**, 104522 (2016).
- [15] G. H. Cao and Z. W. Zhu, *Chin. Phys. B* **27**, 107401 (2018).
- [16] F. F. Balakirev, T. Kong, M. Jaime, R. D. McDonald, C. H. Mielke, A. Gurevich, P. C. Canfield, and S. L. Bud'ko, *Phys. Rev. B* **91**, 220505(R) (2015).
- [17] Y. Liu, J. K. Bao, H. K. Zuo, A. Ablimit, Z. T. Tang, C. M. Feng, Z. W. Zhu, and G. H. Cao, *Sci. China Phys. Mech. Astron.* **59**, 657402 (2016).
- [18] H. Z. Zhi, T. Imai, F. L. Ning, J. K. Bao, and G. H. Cao, *Phys. Rev. Lett.* **114**, 147004 (2015).
- [19] J. Yang, Z. T. Tang, G. H. Cao, and G. Q. Zheng, *Phys. Rev. Lett.* **115**, 147002 (2015).
- [20] Y. T. Shao, X. X. Wu, L. Wang, Y. G. Shi, J. P. Hu, and J. L. Luo, *Europhys. Letts* **123**, 57001 (2018).
- [21] D. T. Adroja, A. Bhattacharyya, M. Telling, Y. Feng, M. Smidman, B. Pan, J. Zhao, A. D. Hillier, F. L. Pratt, and A. M. Strydom, *Phys. Rev. B* **92**, 134505 (2015).
- [22] G. M. Pang, M. Smidman, W. B. Jiang, Y. G. Shi, J. K. Bao, Z. T. Tang, Z. F. Weng, Y. F. Wang, L. Jiao, J. L. Zhang, J. L. Luo, G. H. Cao, and H. Q. Yuan, *J. Magn. Magn. Mater.* **400**, 84 (2016).
- [23] H. K. Zuo, J. K. Bao, Y. Liu, J. H. Wang, Z. Jin, Z. C. Xia, L. Li, Z. Xu, J. Kang, Z. W. Zhu, and G. H. Cao, *Phys. Rev. B* **95**, 014502 (2017).
- [24] C. Cao, H. Jiang, X. Y. Feng, and J. H. Dai, *Phys. Rev. B* **92**, 235107 (2015).
- [25] L. D. Zhang, X. M. Zhang, J. J. Hao, W. Huang, and F. Yang, arXiv:1809.07117.
- [26] Q. Li, M. X. Wang, T. Liu, Q. G. Mu, Z. A. Ren, and S. Y. Li, *Acta Phys. Sinica* **67**, 207411 (2018).
- [27] C.-R. Hu, *Phys. Rev. Lett.* **72**, 1526 (1994).
- [28] S. Kashiwaya, Y. Tanaka, M. Koyanagi, H. Takashima, and K. Kajimura, *Phys. Rev. B* **51**, 1350 (1995).
- [29] Y. Tanaka and S. Kashiwaya, *Phys. Rev. Lett.* **74**, 3451 (1995).
- [30] J. Y. T. Wei, N.-C. Yeh, D. F. Garrigus, and M. Strasik, *Phys. Rev. Lett.* **81**, 2542 (1998).
- [31] H. Aubin, L. H. Greene, Sha Jian, and D. G. Hinks, *Phys. Rev. Lett.* **89**, 177001 (2002).
- [32] G. Deutscher, *Rev. Mod. Phys.* **1**, 77 (2005).
- [33] G. Sheet, S. Mukhopadhyay, and P. Raychaudhuri, *Phys. Rev. B* **69**, 134507 (2004).
- [34] G. E. Blonder, M. Tinkham, and T. M. Klapwijk, *Phys. Rev. B* **25**, 4515 (1982).
- [35] R. S. Gonnelli, D. Daghero, G. A. Ummarino, V. A. Stepanov, J. Jun, S. M. Kazakov, and J. Karpinski, *Phys. Rev. Lett.* **89**, 247004 (2002).
- [36] R. C. Dynes, V. Narayanamurti, and J. P. Garno, *Phys. Rev. Lett.* **41**, 1509 (1978).